WRINKLED MEMBRANES
PART III: NUMERICAL SIMULATIONS

Y. Wesley Wong and Sergio Pellegrino

WRINKLED MEMBRANES
PART III: NUMERICAL SIMULATIONS

Y. WESLEY WONG AND SERGIO PELLEGRINO

This is the third and final part of a study of wrinkles in thin membrane structures. High-fidelity, geometrically nonlinear finite element models of membrane structures, based on thin-shell elements, are used to simulate the onset and growth of wrinkles. The simulations are carried out with the ABAQUS finite element package. The accuracy of the results is demonstrated by computing the characteristics of the wrinkles in two specific membrane structures that were investigated experimentally and analytically in the first two papers in this series.

1. Introduction

This is the third and final part of a study of wrinkles in thin membrane structures. High-fidelity, geometrically nonlinear finite element models of membrane structures, based on thin-shell elements, are used to simulate the formation and growth of wrinkles.

Previous numerical studies of wrinkled membranes have largely focussed on determining the region(s) affected by wrinkles and the direction of the wrinkles. It is now possible to compute the actual shape and size of the wrinkles in structures of realistic shape and size. Here we present a general procedure for carrying out such simulations using the commercially available finite element package ABAQUS [ABAQUS 2001]. The effectiveness of the proposed procedure is demonstrated by computing the wrinkle details of two particular membrane structures, which we had investigated in detail, both experimentally and analytically [Wong and Pellegrino 2006a; 2006b]. It is shown that the accuracy of the wrinkles computed in this way is such that the numerical simulation can now be seen as a replacement for physical experimentation, although the computer run times are currently still impractically long for the present procedure to be adopted as a design tool. A significant, immediate benefit of the present work is that one can probe the simulation results in order to gain additional insights into the characteristics of wrinkles and their evolution under varying loads or boundary conditions.

The layout of the paper is as follows. The next section presents a brief review of previous numerical studies of membrane wrinkling, including a few, recent studies that have adopted shell-based models of the membrane.

Section 3 sets out the proposed finite element procedure. The membrane is represented with a fine mesh of thin-shell elements; first it is lightly prestressed, then a buckling analysis is done to determine a number of incipient buckling modes, which are then seeded as initial imperfections for the main, geometrically nonlinear wrinkling analysis. An alternative model is presented in Section 4. Here the structure is represented by membrane elements and an essentially two-dimensional no-compression elastic solution is sought by means of an iterative procedure that alters the effective Poisson's ratio in order to eliminate any compressive stresses (solutions obtained from this membrane model were used as a reference in [Wong and Pellegrino 2006b], to compare with the analytical solutions presented there).

Section 5 presents a study of a rectangular membrane in simple shear. First, the sensitivity of the wrinkle details to the magnitude of the seeded imperfections, the type of finite elements and the mesh density used for the simulation are investigated. Next, the overall response of the membrane is studied, including the characteristics of the wrinkles. Finally, the way the wrinkles change with the shear displacement is investigated, and it is found that the number of wrinkles changes suddenly, both when decreasing or decreasing the old displacement. The mechanism through which new wrinkles are created, or wrinkles disappear, is explained.

Section 6 presents a study of a square membrane that is pulled at the corners. This problem is representative of currently proposed applications of membranes in future spacecraft structures, and has already been examined from an experimental and analytical viewpoint in the previous two papers in this series. Here the finite element simulation is shown to capture both of the wrinkling regimes that had been observed in the experiments, and details of the corresponding stress distributions are also obtained.

Section 7 discusses the outcomes of the present study and concludes the paper.

2. Review of previous numerical studies

The vast majority of all previous numerical solutions of wrinkled membranes have adopted a purely in-plane model of the structure, hence assuming that bending stresses are negligibly small. This approach will be reviewed first. It can accurately predict the stress distribution in the membrane, including wrinkled regions, and also the extent of these regions, but it provides no information on wrinkle details. An alternative approach is to model the membrane as a thin shell; recent work along these lines will be reviewed in the latter part of this section.

2.1. *Models using membrane elements.* The first finite element solution to incorporate wrinkling theory was the *Iterative Materials Properties* model (IMP) developed in [Miller and Hedgepeth 1982; Miller et al. 1985]. It is based on the observation that if during a simulation a membrane element is deemed to be wrinkled, the geometric strain in the direction perpendicular to the direction of the wrinkles, due to out-of-plane deformation of the material, can be modelled by introducing a variable effective Poisson's ratio for the element.

Hence, instead of using the standard "taut" modulus matrix, based on Hooke's law for plane stress and given by

$$D_t = \frac{E}{1-\nu^2} \begin{bmatrix} 1 & \nu & 0 \\ \nu & 1 & 0 \\ 0 & 0 & \frac{1}{2}(1-\nu) \end{bmatrix}.$$

Miller et al. used the "wrinkled" modulus matrix

$$D_w = \frac{E}{4} \begin{bmatrix} 2(1+P) & 0 & Q \\ 0 & 2(1-P) & Q \\ Q & Q & 1 \end{bmatrix},$$

where $P = (\epsilon_x - \epsilon_y)/(\epsilon_1 - \epsilon_2)$ and $Q = \gamma_{xy}/(\epsilon_1 - \epsilon_2)$; $\epsilon_x, \epsilon_y, \gamma_{xy}$ are the engineering components of plane strain; ϵ_1, ϵ_2 are the major and minor principal strains ($\epsilon_1 \geq \epsilon_2$); and the directions 1 and 2 are parallel and perpendicular to the wrinkles, respectively. For later on, note that σ_1, σ_2 are the major and minor principal stresses ($\sigma_1 \geq \sigma_2$).

Adler [2000] implemented this model as a user-defined material (UMAT) subroutine in the ABAQUS finite element package [ABAQUS 2001]. At any stage of a standard ABAQUS iteration Adler's IMP subroutine begins by calculating the principal strain and stresses at any point using D_t, initially assuming the element to be taut, and then checks:

- If $\sigma_2 \geq 0$, the element is taut and so no change is needed;
- If $\sigma_2 < 0$ and $\epsilon_1 \leq 0$, the element is slack and so all stress components are zero;
- If $\sigma_2 < 0$ and $\epsilon_1 > 0$, the element is wrinkled, so the stress components are recomputed using D_w.

This is known as the *combined wrinkling criterion*, as a combined stress/strain condition has to be satisfied for a wrinkle to exist. Wrinkling criteria based purely on stress or strain have potential shortcomings and are less accurate [Kang and Im 1997; Liu et al. 2001].

Successful predictions of the shape and pattern of the wrinkled regions in a square membrane subjected to point loads, and also in inflated balloons of different

shapes were obtained by Adler [2000]. The main problem was that the solution tended to diverge in the presence of many slack regions.

Johnston [2002] used the same approach to analyse the static and dynamic behaviour of the sunshield for a space telescope. This sunshield consists of several reflective foils which wrinkle extensively.

An alternate tension field model was developed by Liu et al. [1998] and incorporated into the nonlinear finite element code TENSION6. The main difference between this method and IMP is that, instead of modifying the material properties iteratively, the user preselects a so-called penalty tension field parameter to provide a small amount of stiffness in the direction transverse to the wrinkles. This helps to overcome the numerical singularities associated with vanishingly small diagonal terms in the tangent stiffness matrix. Liu et al. [1998] carried out a simulation of the deployment of a parachute. Modelling issues, including the selection of the penalty term, influence of the order of integration and local remeshing in the wrinkled regions are all discussed in this paper.

Liu et al. [2000] combined the approach of their earlier paper with the semianalytical determination of the impending buckling mode by Lin and Mote [1996]. The resulting two-level analysis is able to determine both the extent of the wrinkled regions, by determining the stress field with TENSION6, and the wrinkle wavelength and amplitude, by applying Lin and Mote's eigenvalue analysis to determine the number of wrinkles. The wrinkle amplitude is then determined through an argument essentially equivalent to that put forward in [Wong and Pellegrino 2006b, Section 4]. It is implicitly assumed that the number of wrinkles will not vary once the wrinkles have started to form (which is not correct), and that the wrinkled region can be assumed to behave as a simply supported rectangular plate. Liu et al. [2000] have shown this approach to provide reasonably accurate results for a square membrane subjected to a specific combination of tension and shear.

Several iterative schemes that use no-compression material models have been proposed. In their simplest form, these schemes begin by assuming that the behaviour of the membrane is linear elastic. Then, any compressive principal stresses are set to zero and the associated stiffness matrix coefficients are also set to zero. The principal stresses are recalculated at every iteration, to avoid history dependency in the results. An early study of airbag inflation based on this approach [Contri and Schrefler 1988] set a sample problem that many others have subsequently tackled. An analogous approach was attempted by the present authors, using the *NO COMPRESSION option in ABAQUS, but poor convergence was observed.

Finally, a number of membrane finite elements that incorporate wrinkling within their formulation have been derived from a continuum mechanics approach. The methods proposed range from using a modified deformation tensor [Roddeman

et al. 1987], to a geometrically modified [Nakashino and Natori 2005] or energetically modified [Haseganu and Steigmann 1994; Barsotti and Ligaro 2000] stress-strain tensor.

2.2. *Models using shell elements.* Tomita and Shindo [1988] were the first to make use of a three-dimensional shell description of a wrinkled membrane, in a study of the residual wrinkles in a thin metallic plate that has been pulled diagonally. This paper started with an analysis of the onset of wrinkling, which was assumed to be the outcome of a bifurcation from plane deformation to out-of-plane deformation of the plate. The plate was initially represented by a mesh of thin-plate elements, including the effects of material nonlinearity, but the growth of the wrinkles was then traced by switching the model to isoparametric shell elements.

The last five years have seen regular use of the ABAQUS package, and recently also of ANSYS [ANSYS 2000], to simulate the onset of wrinkling in a tensioned strip [Friedl et al. 2000] and the growth of wrinkles. Three approaches to the simulation of wrinkle growth have been proposed, differing in the way the out-of-plane deformation is triggered at the beginning of a geometrically nonlinear analysis. In [Wong and Pellegrino 2002a] and [Wong et al. 2003] we started by extracting a set of eigenvalues/eigenvectors of the tangent stiffness matrix of the structure. Instead, Leifer and Belvin [2003] applied a set of equal and opposite, small magnitude forces perpendicular to the membrane and with a resultant of zero. Finally, Tessler et al. [2003; 2004] and Papa and Pellegrino [2005] imposed randomly distributed, out-of-plane imperfections, of similar magnitudes to those imposed in [Wong and Pellegrino 2002a].

The choice of finite elements and the type of analysis procedure are essentially equivalent in the three simulation techniques (the details are explained in Sections 3 and 5), so the key difference between the first approach and the other two is the additional burden of the initial eigenvalue/eigenvector extraction. In the present study it was found that this additional computation requires only a small fraction of the total simulation time, hence this burden is not significant. The three approaches have been tested on similar problems and found to work equally well for a membrane under shear, where the wrinkles are relatively uniform. For a membrane under equal corner loads the agreement between experiments and results from eigenvector-based perturbations, presented in this paper, is better than the latest results with random imperfections; see Tessler et al. [2005, Figure 5].

3. Three-dimensional finite element models

The bending stiffness of a membrane, although small, plays a key role in determining the shape and amplitude of the wrinkles. Therefore, it is essential that it should be included in any models that aim to capture this kind of detail. Two options are

available, first to model the membrane with thin-plate elements and second to use thin-shell elements. Since the first option would only work for flat or nearly flat membranes, the second option has been pursued.

ABAQUS offers several shell elements, and preliminary runs were carried out with 3-node triangular and 4-node quadrilateral general purpose elements with full integration (S3, S4); these elements have six degrees of freedom at each node. 4-node and 9-node reduced integration, thin-shell elements (S4R5, S9R5), with five degrees of freedom per node, were also investigated. ABAQUS also provides other shell elements which are mainly suited for thick shell problems. This is a different class of problem and no detailed investigation of these elements was carried out.

The S3 element uses constant bending curvature and membrane strain approximations; therefore a very fine mesh is required to capture the bending deformation due to wrinkling. Note that the fineness of the discretisation that is required is related to the expected wrinkling wavelength. The formulation of element S4 is similar to S3 for bending, but the in-plane strain field has been enhanced to eliminate shear locking effects. Both S4R5 and S9R5 are thin shell elements with three in-plane translations and two in-plane rotation components. They use reduced integration with hourglass control to avoid shear locking. Both elements can model thin shells fairly accurately and S4R5 was chosen since it is computationally more economical. A detailed comparison of the performance of different shell elements in the analysis of a shear membrane will be presented in Section 5.1.2.

After defining the finite element mesh, type of elements, and material properties, a wrinkling analysis employing thin shell elements is typically performed in three stages, as follows.

3.1. *Initial conditions.* The initial stage of the analysis applies a small uniform prestress to the membrane, to stabilize it. Several strategies can be used to apply this initial prestress. One technique is to prescribe a set of edge displacements, corresponding to the level of prestress required. This technique is particularly useful for setting up the true stress state of a membrane structure, e.g. to reproduce the conditions that may exist at the beginning of a test. However, if a uniform stress state is required instead, e.g. to avoid initial numerical singularities, this simpler prestress can be obtained more readily by prescribing a set of initial stresses using the *INITIAL CONDITIONS, TYPE=STRESS parameter in ABAQUS. In the latter case, only membrane forces, bending moment and twisting moments can be specified for shell elements.

After applying the initial prestress, a static, geometrically nonlinear equilibrium check (*STATIC, NLGEOM) is performed. This check induces a small re-distribution of the state of prestress, together with small in-plane displacements.

3.2. *Eigenvalue/eigenvector extraction.* The next step of the analysis determines the buckling mode-shapes of a lightly prestressed membrane. These modes are then used as small, initial imperfections that trigger the formation of wrinkles in the subsequent, geometrically nonlinear simulation.

An eigenvalue buckling analysis (*BUCKLE) is used to obtain the possible wrinkling modes of the membrane subjected to its actual boundary conditions and loading. The loading is typically defined in terms of a set of applied forces or displacements at the edge of the membrane, and has to represent the loads on the real structure. It is important that both the initial stresses and displacements from the previous stage of the analysis, as well as those due to the applied load, should be included in the calculation of the tangent stiffness matrix; ABAQUS performs these calculations by default. The eigenvalues and eigenvectors of the tangent stiffness matrix correspond to the load magnitudes and shapes of the possible wrinkling modes of the membrane. Two solvers are available in ABAQUS to extract the eigenvalues, namely subspace iteration and the Lanczos method. The default, subspace iteration method is generally quicker when only a few (typically, less than 20) eigenmodes are needed.

After computing the buckling mode-shapes, a linear combination of all, or some selected eigenmodes is introduced into the structure as a geometrical imperfection. In standard buckling analysis of imperfection-sensitive structures, the imperfections that are seeded in the structure are normally obtained as linear combinations of the eigenvectors corresponding to the lowest eigenvalues. However, the main objective of the present study is not finding the lowest eigenvalue, corresponding to the load which would cause the first wrinkle to form. The first wrinkle forms almost as soon as the load is applied, but we are interested in following the evolution of this first wrinkle, leading to the formation of a second one, and so on until a large number of wrinkles have formed. It is generally best to introduce in the membrane a rather general kind of imperfection, e.g. one obtained as the combination of many eigenvectors. In cases where some features of the final wrinkling pattern are known, introducing in the imperfection mode shape eigenmodes that resemble this pattern, as well as several other eigenmodes, generally increases the speed of convergence during the initial stages of the simulation.

Once a set of eigenmodes has been chosen, geometrical imperfections are introduced in the form of out-of-plane deformations of the membrane, using the *IMPERFECTION directive:

$$\Delta z = \Sigma_i w_i \phi_i,$$

where w_i is the i-th eigenmode and ϕ_i is a scaling factor whose magnitude is chosen as a proportion of the thickness of the membrane. Values between 1% and 100%

of the thickness have been used, and the sensitivity of the predicted response to different ϕ_i's has been determined, see Section 5.1.1.

3.3. *Simulation of wrinkle growth.* A geometrically nonlinear (*NLGEOM) incremental analysis is carried out under edge displacement incrementation, using the Newton–Raphson solution method. Since the equilibrium path of a wrinkled membrane includes many unstable branches, each corresponding to a localised snap-through due to the formation of an additional wrinkle, the only type of solution algorithm able in theory to compute the full response of the structure is an arc-length solution. The full response of the structure cannot be computed by increasing monotonically a single displacement parameter, but all attempts to use the arc-length solution method in ABAQUS (*RIKS) were unsuccessful, possibly because wrinkling is a highly localised type of instability. Hence, monotonic displacement incrementation was the only viable option.

A very effective way of addressing the numerical singularities associated with an instability is to switch from a quasi-static simulation to a transient dynamic analysis. Thus, one would simulate the actual dynamic response of the structure as it snaps, in order to compute the first static equilibrium state after snapping has occurred. This idea can be straightforwardly implemented in ABAQUS using the STABILIZE function. However, instead of computing the actual dynamics of the snap, when an instability is detected ABAQUS automatically introduces pseudo-inertia and pseudo-viscous forces at all nodes, and switches from a solution of the actual stiffness equations to a solution of a set of pseudo-equations-of-motion.

The default fictitious viscous forces are calculated on the basis of the model's response in the first increment of the analysis step, by assuming that the energy dissipated is a prescribed fraction of the strain energy during the first step. This fraction is called *damping intensity*, or *stabilise factor*, in ABAQUS and has a default value of 2×10^{-4}. To achieve good accuracy, it is generally desirable to set this parameter to the lowest possible value for which convergence can still be achieved.

The flowchart in Figure 1 summarises the complete simulation procedure.

4. Two-dimensional finite-element models

In addition to the model presented in the previous section, that has been used very extensively for the work presented in this paper, a number of comparative two-dimensional analyses were also carried out. In these analyses the structure was modelled with a mesh of membrane finite elements, typically 3-node triangular or 4-node quadrilateral full/reduced integration general purpose elements (M3D3, M3D4, M3D4R). As well as the standard linear-elastic material model, a wrinkled
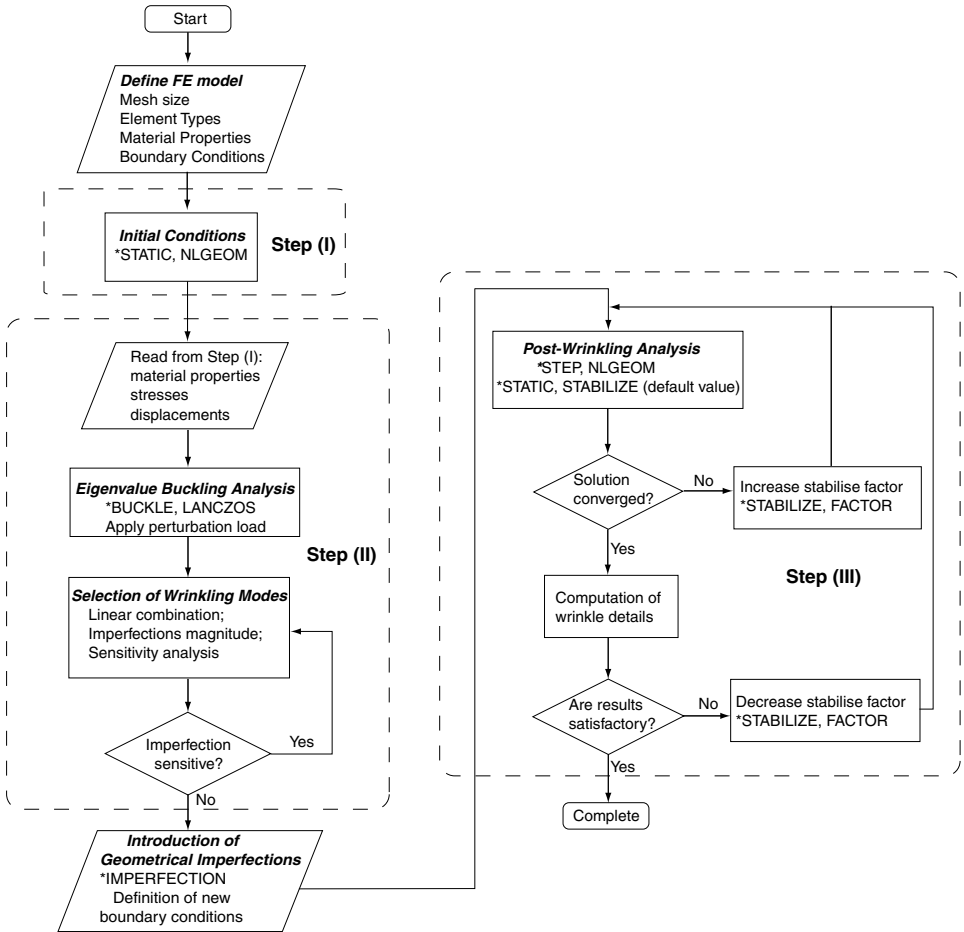
Figure 1. Flowchart for wrinkling analysis using thin shell model.

material definition was implemented through the user-defined material subroutine (UMAT) developed by Adler [2000].

The analysis procedure for the membrane model was similar to that presented in Section 3 for the shell model, but there is no eigenvalue/eigenvector extraction. After setting up the FE model of the structure, using membrane elements, an additional parameter is provided after the *MATERIAL, ELASTIC option USER=IMP.

The model was set up either in two dimensions, by constraining all out-of-plane degrees of freedom, in which case no initial prestress was needed, or in three dimensions, and in this case a small initial prestress was used to numerically stabilise the model, as for the thin-shell model.
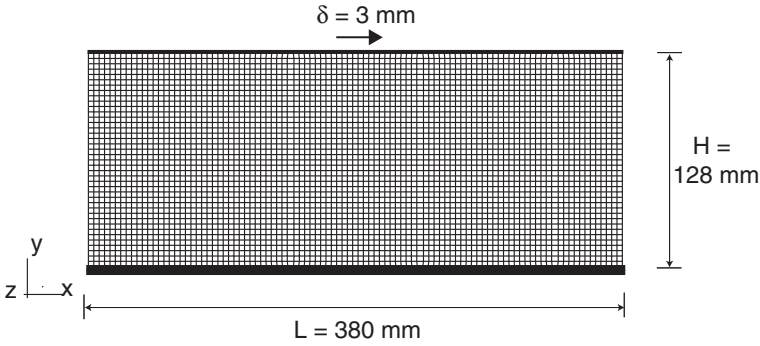
Figure 2. Finite element mesh for membrane in shear.

5. Membrane in simple shear

This section presents a study of the formation and growth of wrinkles in an initially flat and stress-free, linear-elastic rectangular membrane subject to simple shear. The dimensions of the membrane are shown in Figure 2, and the material properties are listed in Table 1.

Figure 2 shows the finite element mesh used for a preliminary analysis that was carried out. It consists of 3960 four-noded quadrilateral S4R5 thin-shell elements; each element has an aspect ratio of approximately one. The analysis started with a relatively fine mesh, in order to properly resolve the wrinkles. The element size was initially set to be smaller than the wrinkle half-wavelength, which in the present problem can be estimated from [Wong and Pellegrino 2006b, Eq. (14)]. Also shown in the figure is the final horizontal shear displacement, $\delta = 3$ mm, of the upper edge of the membrane.

Using the *BOUNDARY, ENCASTRE option, The bottom edge of the membrane was fully constrained. This was the only boundary condition assigned in the model history definition, and so it remained active through all analysis steps. The other boundary conditions were modified during the analysis, as explained in the next section.

Thickness, t (μm)	25
Young's Modulus, E (N/mm^2)	3500
Poisson's ratio, ν	0.31
Density, ρ (kg/mm^3)	1.5×10^{-6}

Table 1. Kapton$^{\circledR}$ membrane properties

The upper edge of the membrane was connected to a series of B21 beam elements, with a 15 mm wide by 30 mm deep rectangular section, $E = 215000$ N/mm^2 and $\nu = 0.35$, modelling the sliding element of the experimental rig used in [Wong and Pellegrino 2006a]. The beam elements were connected to the nodes along the upper edge of the membrane using the multi-point constraint option *MPC, TIE.

5.1. *Simulation details.* Each simulation consisted of three steps, as follows.

The first step consisted in pretensioning the membrane by moving the upper edge by 0.5 mm, in the y-direction. Then, a geometrically nonlinear equilibrium check was performed. The geometric stiffness provided by the prestress has the effect of increasing the out-of-plane stiffness of the thin membrane. Only translation in the y-direction was allowed for the two side edges, and all six degrees of freedom of the bottom edge were completely constrained.

In the second step, an eigenvalue buckling analysis was carried out with a prescribed horizontal displacement of 3 mm at the upper edge. The model boundary conditions were modified by using the *BOUNDARY, OP=MOD option. This has the effect of moving the upper edge nodes in the horizontal x-direction by the prescribed displacement. All degrees of freedom of the nodes along the two side edges were completely free, to simulate the actual situation in the experimental model.

Earlier analyses had shown that the eigenmodes corresponding to eigenvalues smaller than 0.2 correspond to local deformation modes of the membrane (note that this particular value of the smallest eigenvalue depends on the initial prestress applied in the first step), and hence are of limited interest for the wrinkling analysis. Therefore, the Lanczos solver in ABAQUS was set to produce only eigenmodes whose eigenvalues are greater than 0.2. The first four symmetric modes are presented in Figure 3. Note that all of these modes closely resemble the expected wrinkled pattern, i.e., the parallelogram of wrinkles observed experimentally in [Wong and Pellegrino 2006a] and also predicted analytically in [Wong and Pellegrino 2006b]. Also note that all four modes have approximately the same wavelength. The chosen geometrical imperfections were then seeded onto the pristine mesh using the *IMPERFECTION command.

The third and final step consisted of two substeps. First, the initial pretensioning step was repeated, as described earlier, but this time with the upper edge only displaced by 0.05 mm to give an initial prestress of approximately 1.5 N/mm^2. Note that, although in the first step a much higher prestress had been used, in order to avoid the presence of many localised modes in the eigenvalue buckling analysis step, here a smaller prestress is sufficient to provide a small, initial out-of-plane stiffness to the membrane, but without affecting the final results. Then, in the second substep the upper edge was moved horizontally by 3 mm while all other
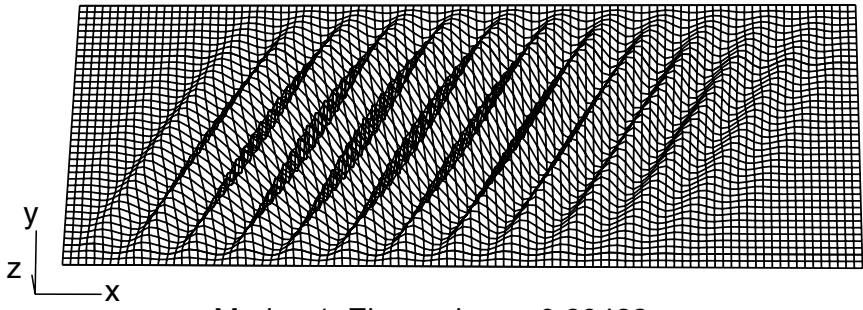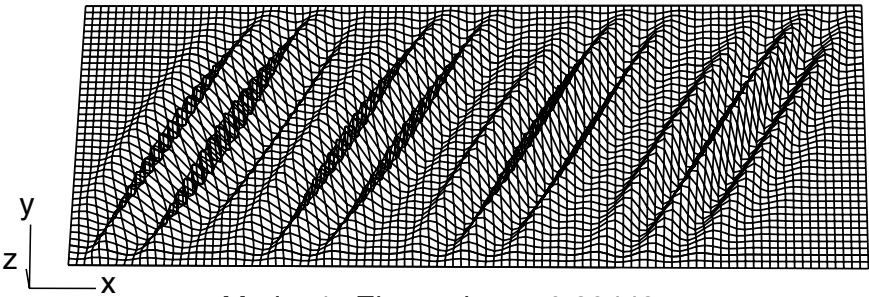
Mode   1: Eigenvalue = 0.20423
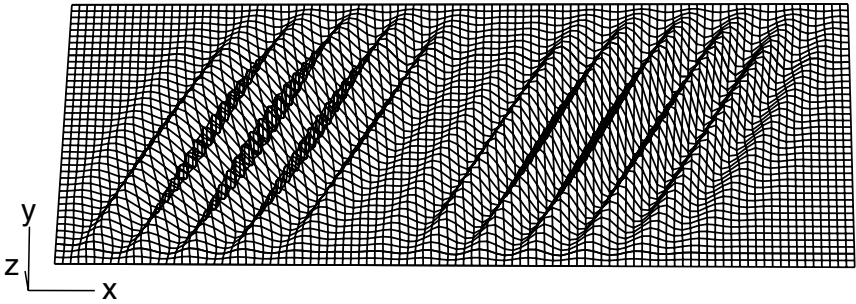
Mode   2: Eigenvalue = 0.20428
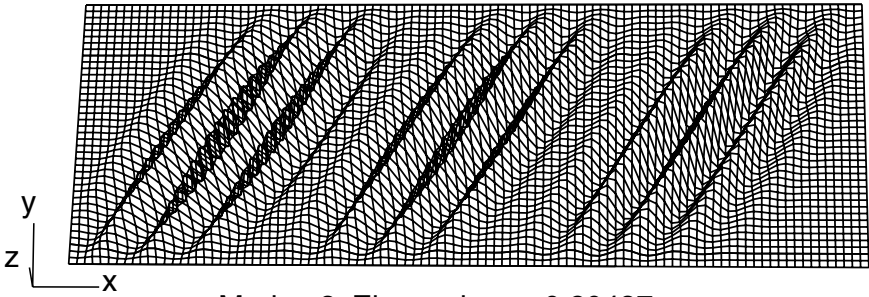
Mode   3: Eigenvalue = 0.20437

Mode 4 : Eigenvalue = 0.20449

Figure 3. First four eigenmodes with eigenvalue > 0.2, for membrane is shear.

degrees of freedom were constrained. All translational degrees of freedom of the side edges were left free, but the rotations were constrained to aid convergence.

The STABILIZE function was activated for this substep. The parameter that controls the amount of numerical damping has the default value 2×10^{-4}. This parameter was adjusted almost continuously, according to the level of difficulty of converging to a solution, by using the *RESTART option. This approach allows the numerical damping to be made very small, to minimise the deviation between the computed equilibrium path and the actual path, and to be increased only when necessary. The smallest factor used in the rectangular membrane simulations was 1×10^{-8} (*STABILIZE, FACTOR = 1E-8) .

5.1.1. *Initial imperfections.* Many different combinations of eigenmodes and scaling factors were considered to test the sensitivity of the results of the detailed wrinkling analysis. For each set, a complete wrinkling simulation was carried out and the maximum and minimum out-of-plane displacements, w_{max} and w_{min}, were computed. A set of sample results are shown in Table 2.

Note that the maximum displacements remain practically unchanged when the magnitude of the imperfections is increased by a factor of 10. Also note that the particular displacements listed in the table correspond to the largest two wrinkles, on either side of the membrane, but the smaller wrinkles between these large ones were also found to have the same amplitude and wavelength, regardless of the size of imperfection.

It was thus concluded that the particular magnitude of the chosen imperfection is not critical. It was decided to use a "standard" imperfection consisting of the first four eigenmodes corresponding to eigenvalues greater than 0.2, normalised to a unit length by ABAQUS, each multiplied by a scaling factor $\phi_i = 0.125t$.

5.1.2. *Comparison of different elements.* After selecting a standard set of imperfections on the basis of a mesh of S4R5 thin shell elements, as described in Section 5.1.1, a detailed study of the performance of different elements was carried out.

Table 3 lists the number of wrinkles n (see Section 5.3), the wrinkle wavelength 2λ, the amplitude A, and the total simulation time for each type of element.

$\phi_1, \ldots, \phi_4$	w_{max} (mm)	w_{min} (mm)
0.025t	1.12	−1.49
0.125t	1.09	−1.49
0.250t	1.14	−1.51

Table 2. Sensitivity of membrane in shear to imperfection magnitudes

Element	S3	S4	S4R5	S9R5	M3D4
n	13	11	16	16	9
2λ (mm)	28.6	33.9	21.2	23.0	42.3
A (mm)	0.651	0.999	0.432	0.453	0.83
CPU (s)	31869	5714	10192	79419	791

Table 3. Number of wrinkles, wavelength, amplitude and total simulation time for different element types, for membrane in shear.

The most important parameter is the total number of wrinkles, since it can be readily compared to the experimental observations. In [Wong and Pellegrino 2006a] we observed 19 wrinkles when a 3 mm displacement was imposed on a 25 mm Kapton® film.

Here, elements S3 and S4 predicted 13 and 11 wrinkles, whereas S4R5 and S9R5 both predicted 16 wrinkles. Note that S3 failed to converge with the specified stabilize factor of 1×10^{-8}; the results presented in Table 3 were obtained by specifying a damping factor of 5×10^{-3}. The membrane element M3D4, with a standard linear-elastic material model, predicted only 9 wrinkles.

Hence, elements S4R5 and S9R5 match the experimental results most closely. Since S4R5 is superior in terms of computational efficiency and economy, it was adopted for all the following analyses.

5.1.3. *Sensitivity to mesh density.* The initial mesh, shown in Figure 2, predicted a smaller number of wrinkles than that observed in the experiment. Therefore, two additional mesh sizes were used to investigate the effect of mesh density on the final wrinkled shape.

The two meshes consisted of 6950 and 13134 elements, approximately double and four times the number in the initial mesh. Both of the denser meshes predicted the same number of wrinkles as in the experiment (Table 4), which suggests that the solution becomes mesh-independent after a particular level of refinement.

No. elements	Total dof	No. wrinkles
3960	19800	17
6950	34750	19
13134	65670	19

Table 4. Dependence of number of wrinkles on mesh density.
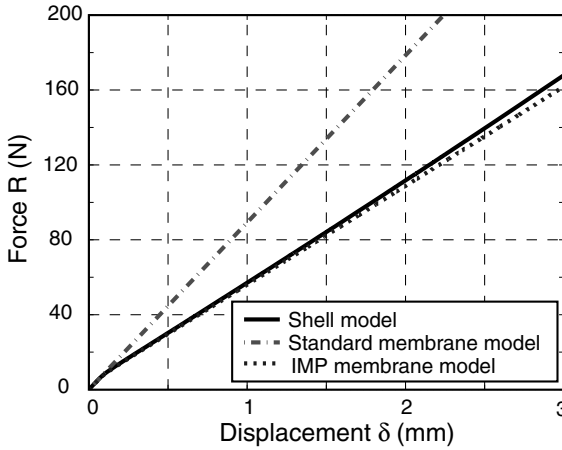
Figure 4. Shear force-displacement relationship, for membrane in shear.

Since the computational time increases roughly proportionally to the number of elements, the mesh with 6950 S4R5 elements was selected. The results presented and discussed from now on are all based on this model.

5.2. *Global behaviour of wrinkled membrane.* The overall relationship between the total shear force applied to the membrane and the shear displacement, δ, has been computed using three different models; the results are shown in Figure 4. Both the shell model and the IMP membrane model predict an initial in-plane shear stiffness of 101 N/mm, which quickly decreases by about a third as the wrinkles begin to form. Afterwards, the response is essentially linear. The membrane model with standard, linear-elastic material does not capture the softening associated with the formation of wrinkles (although a certain amount of waviness is created as a result of the initial imperfections).

A vector plot of the midsurface stress distribution (obtained from the shell model) corresponding to the final displacement $\delta = 3$ mm is shown in Figure 5. For each element, the directions and magnitude of the two principal stresses have been plotted, but the major stress, σ_1, is so much larger than the minor stress, σ_2, that only one vector can be seen. The direction of the major principal stress corresponds to the direction of the wrinkles, which are clearly uniform and inclined at 45° in the central part of the membrane. There are two lightly stressed triangular regions near the side edges, and the top right and bottom left corners act as stress risers, with stress concentrations of up to 2.5 times the average stress.

Figure 6 shows the overall, final wrinkle pattern in the membrane. The wrinkles in the central region are at 45° to the edges, but near the pair of corners that move closer together the wrinkles are "pinned" and hence form a kind of fan region.

A deeper understanding of the stress distribution in the wrinkled membrane can be obtained by considering the principal stresses across the midheight section, at $y = 64$ mm, defined by the section line A-A in Figure 6. Figure 7 shows plots of the major and minor principal stresses through the midplane of the membrane for two values of the shear displacement. The plots show that σ_1 increases rapidly, starting from zero at the edges, to an approximately uniform, positive value, whereas σ_2 remains very small. Close inspection shows this value to be always negative and roughly uniform across most of the section.

5.3. *A closer look.* The linearity of the overall load-deflection response computed in Section 5.2 hides some interesting instabilities, which become apparent on closer inspection. When the shear displacement is gradually and monotonically increased, the existing set of wrinkles grow in amplitude, then become unstable and give rise to an extra wrinkle, and hence all of the wrinkles suddenly have a smaller wavelength and amplitude, and then the cycle repeats.

50 N/mm2
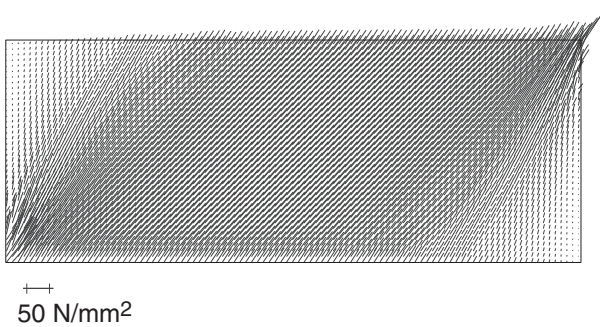
Figure 5. Plot of principal stress directions and magnitudes, for membrane in shear, showing that the major principal stress is (i) uniformly at 45° in the centre region and (ii) about three times larger near the top right and bottom left corners.
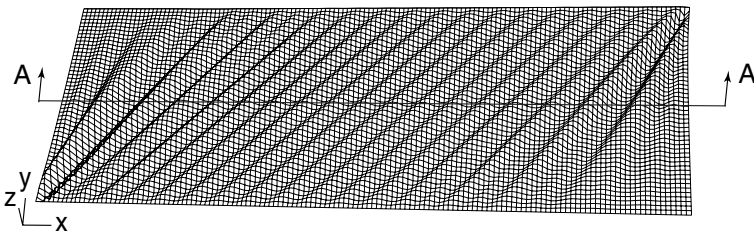
Figure 6. Perspective view of wrinkle pattern, for membrane in shear with $\delta = 3$ mm.
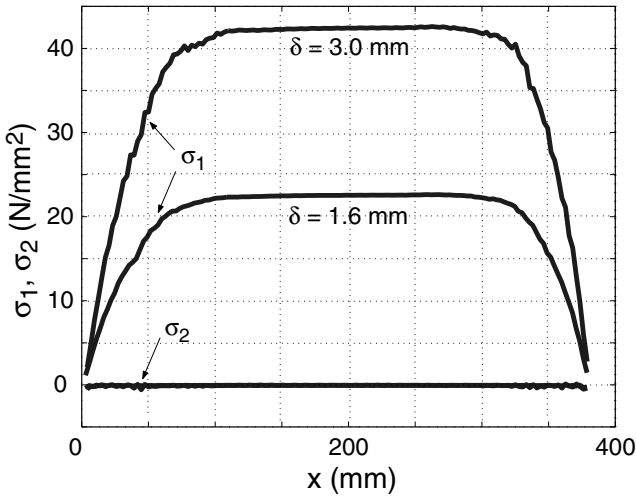
Figure 7. Principal midplane stresses across section A-A of membrane in shear.
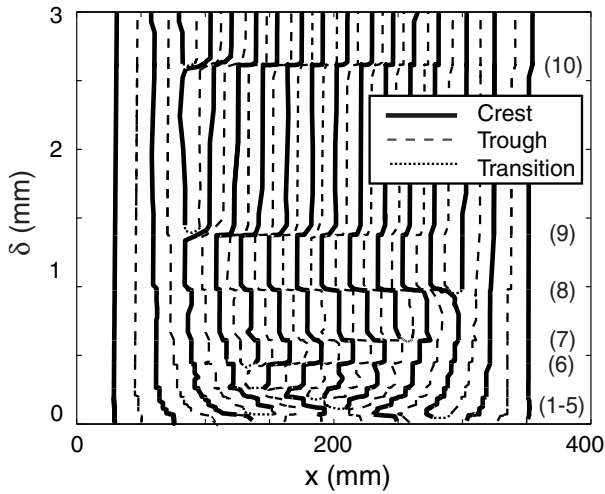
Figure 8. Trajectories of $w_{\max}$ (crest) and $w_{\min}$ (trough), for membrane in shear.

A complete history of how the wrinkle pattern grows is shown in Figure 8. This figure is a plot of δ versus the position of the points of maximum and minimum out-of-plane displacement, i.e. the crests and troughs of the wrinkles, across the midheight section of the membrane.

Note that the solid lines on the two sides of the plot are practically straight and vertical, indicating that the edge wrinkles do not move. Looking further towards the centre of the plot, the first dotted line and the second solid line are continuous, but gently curved outwards. Many other lines contain one or more bifurcation points, which indicate that additional wrinkles are created. The first five bifurcations occur very quickly, at the start of the simulation; afterwards the values of δ associated with each jump can be clearly identified, and are labelled (6)–(10) on the right-hand side of the figure. As the number of wrinkles increases, the membrane becomes more stable and hence a greater increase of δ is required for the next bifurcation to occur.

Because the wrinkles can most easily reorganise themselves in the middle of the membrane, new wrinkles tend to appear close to the edges. The large wrinkles on the sides do not move; they are "pinned" at the corners, as already noted.

Figure 9 shows the different shapes of the midheight section of the membrane, for increasing δ's. The particular shapes shown here were obtained immediately after the bifurcations labelled (2), (4), (6), (7), (9) and (10) in Figure 8. The number of wrinkles, n, defined as the number of crests in each plot, is 9, 11, 13, 14, 16 and 17 respectively. The outermost crest at each side is not counted. Note that the wrinkle amplitude in the central region increases from 0.13 mm to 0.33 mm in these plots, while the wavelength decreases visibly.

5.4. *Mode jumping.* The sudden transitions from one wrinkled shape to another, noted in the previous section, were observed experimentally in [Wong and Pellegrino 2006a]. Each change in the number of wrinkles is a mode jump in the post-buckling response of the membrane.

Mode jumping in stiffened panels under compression has been studied in depth by Stein [1959b; 1959a]. A key difference is that, whereas in Stein's work mode-jumping clearly showed in the load-shortening curves for the panels, here the load-deflection curve is linear, as seen in Figure 4. The reason is that each mode-jump is associated with a change of compressive stresses in the membrane, but their magnitude is negligibly small in comparison with the tensile stresses in the membrane.

Mode jumps have been explained in terms of the interaction of the branches of a set of bifurcation points adjacent to the critical load [Riks 1998]. For the present study, the sequence of jumps is seen most clearly in a plot of the *minor* principal stress, σ_2, versus the shear displacement at a representative point of the membrane. For example, Figure 10 shows the stresses at three points near the centre of the membrane. Which particular point is chosen is not significant, but jumps that are associated with an instability that is distant from the chosen point might not show, therefore we have monitored the stress at several points and chosen three after
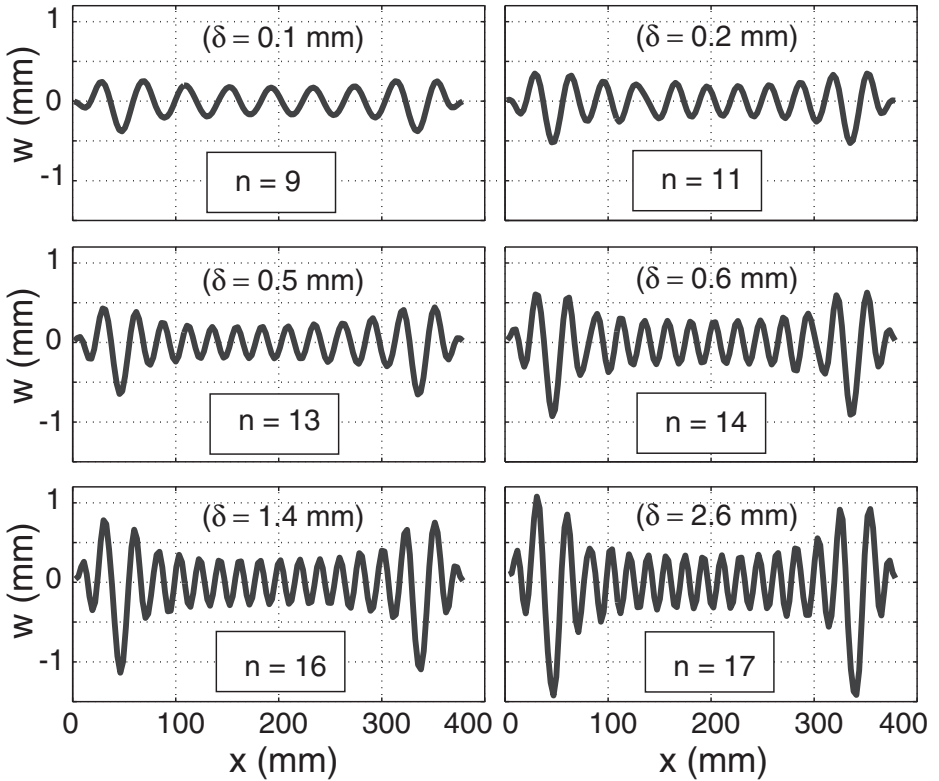
Figure 9. Mid-height cross-sections for different δ's.

completing the analysis. Note that σ_2 is always compressive, and far smaller in magnitude than the tensile stresses plotted in Figure 7.

The stress jumps numbered (1)–(10) in Figure 10 are the same that were investigated in Section 5.3. Jump (1) occurred almost immediately after beginning to increase δ. This jump was facilitated by the initial geometric imperfections. Due to these imperfections, the first jump is directly into a configuration with $n = 7$ wrinkles. This jump is followed in rapid sequence by jumps (2)–(5); and then the membrane settles in a relatively stable configuration. It is interesting to note that, as the membrane becomes more stable, σ_2 remains almost constant between consecutive jumps.

Next, we discuss jump (6) in more detail. Figure 11 shows a sequence of cross-sections of the membrane, corresponding to the 8 points labelled (a-h) on the enlarged part of Figure 7. Figure 11(a-b) shows a 13-wrinkle shape that remains stable until σ_2 has almost reached a peak, at point (c). Here a small asymmetry begins to appear in the cross-sectional plot, which rapidly grows into a new wrinkle (d-e).

Thus, the transition from 13 to 14 wrinkles occurs over a very small increment of
δ. Then the new mode becomes stable and the magnitude of σ_2 starts to decrease.

It is also interesting to simulate a loading-unloading cycle. Figure 12 is a plot
of the variation of the number of wrinkles when δ is increased from 0 to 3 mm,
and then decreased to 0, and finally increased again to 3 mm. Note that during
unloading *the wrinkles tend to stay on*, thus the final number of wrinkles does not
start decreasing until the shear displacement has been reduced to $\delta = 0.8$ mm. At
this point the number of wrinkles suddenly decreases from 17 to 14. Thus, the
behaviour upon unloading is different from that upon loading.

During reloading the membrane generally follows the same path as during the
initial loading, however the final configuration with 17 wrinkles is achieved slightly
earlier this time. This difference may be due to the effect of the geometrical im-
perfections left in the membrane at the end of the first load cycle, which may have
facilitated the formation of the "correct" pattern of wrinkles. Also note that the
stabilise factor was continuously adjusted during each simulation, and also during
load reversal; it is difficult to quantify the effect of this variation.

6. Square membrane under corner loads

This section presents a study of wrinkles in an initially stress free and perfectly
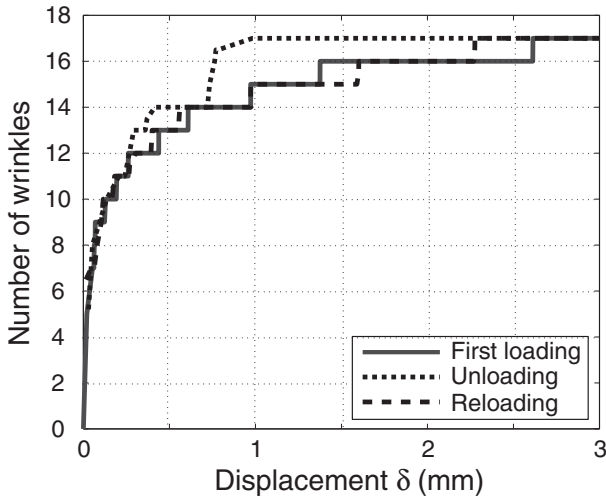flat square membrane, pulled at the four corners by two diagonal pairs of equal
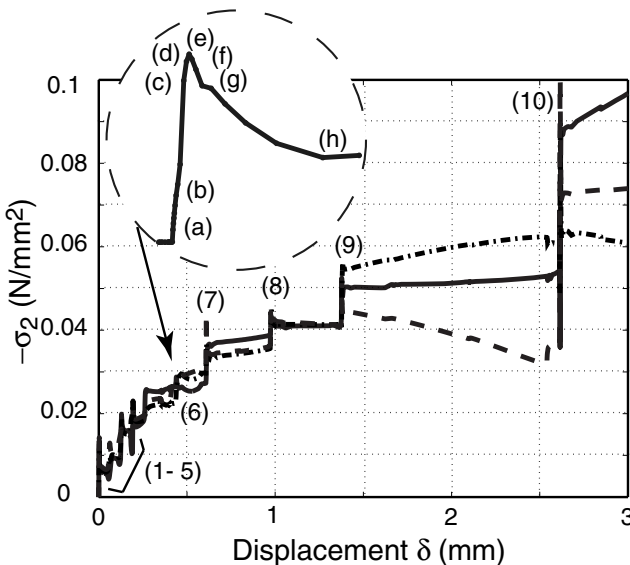
Figure 10. Variation of minor principal stress at three points near
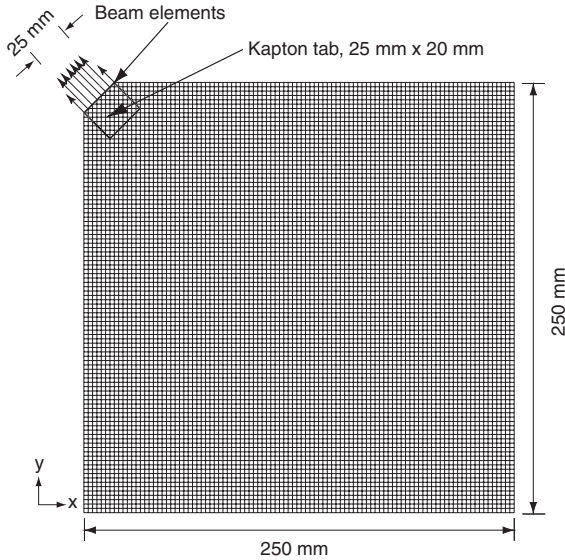centre of membrane under shear.

and opposite forces, T_1 and T_2. Its dimensions are defined in Figure 13 and the material properties are given in Table 1.
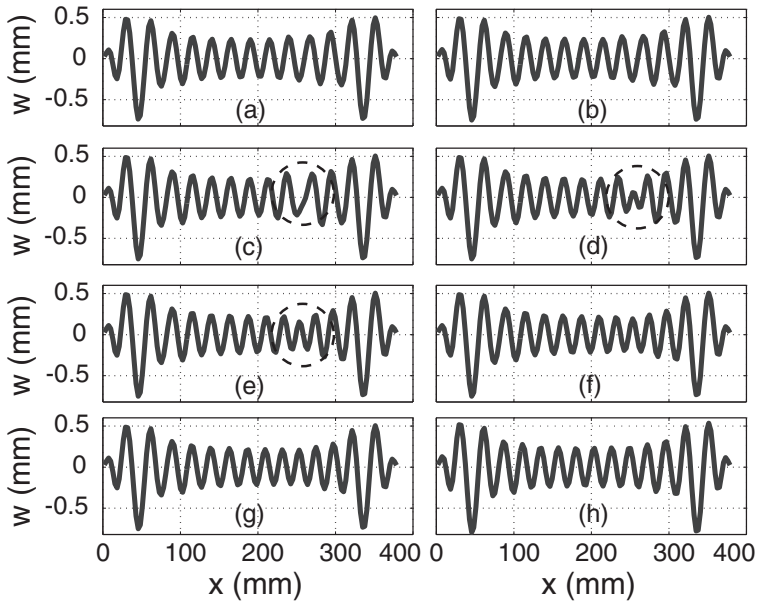
Figure 11. Variation of midheight cross-section during jump (6).

Figure 12. Number of wrinkles during load cycling.

Figure 13. One quarter of the finite element mesh square membrane.

The corners of the square are truncated, to model the actual corners of the experiment in [Wong and Pellegrino 2006a]. They have a width of 25 mm, as shown in Figure 13.

6.1. *Simulation details.* The membrane and corner tabs were modelled using S4R5 thin shell elements of different thicknesses. The corner beams were modelled using beam elements with the Circ general beam section. The *MPC, TIE function was used to connect each beam node to the corresponding shell element node. The membrane was constrained in both *x* and *y*-directions at the centre node; all four side edges were left free; the *z*-translations and all rotational degrees of freedom of the corner beam nodes were restrained. The corner loads were distributed uniformly over the nodes of the beams (with only half of the forces applied at the end nodes).

The analysis procedure was essentially identical for all of the simulations. First, a uniform prestress of 0.5 N/mm^2 was applied to provide some initial out-of-plane stiffness to the membrane. This was achieved by using the *INITIAL CONDITION, TYPE=STRESS parameter in ABAQUS. A nonlinear geometry analysis was then carried out, with the *NLGEOM option activated, to check the equilibrium of the system with this initial prestress.

Second, an eigenvalue/eigenvector extraction was carried out. Many global mode-shapes were selected, and were then superposed — each multiplied by the scaling factor $\phi_i = 0.025t$ — and introduced as an initial geometrical imperfection

at the start of the final analysis step. A smaller value of ϕ_i was chosen for the square membrane than for the rectangular membrane, because it had been found that this configuration is more sensitive to the magnitude of the initial imperfection, particularly at lower stress levels.

Third, an automatically stabilised nonlinear simulation of wrinkle growth was performed. Because the wrinkle amplitude is initially very small, the increment step was set equal to 0.001 of the total load. The *stabilize factor* was set to 10^{-12}, to minimize the effect of numerical damping on the final solution; this value was found to be sufficient for convergence. Despite the initial symmetry of the perfect structure, note that the imperfections are not symmetric and so the whole structure was analysed.

The loading of the membrane was applied in two steps. The first step involved a symmetric loading, $T_1 = T_2 = 5$ N, applied at all corners. Then, T_2 was maintained constant at 5 N while T_1 was increased up to 20 N, corresponding to a final load ratio of $T_1/T_2 = 4$. The second load step was carried out as a follow-on to the first step. Without changing the boundary conditions, T_1 was increased to 20 N by using the *LOAD, OP=MOD command while keeping T_2 constant at 5 N.

No separate eigenvalue extraction was carried out for the second load case, as it was found that the out-of-plane deformation at the end of the first load step naturally develops into the wrinkled profile for the second step. Also note that the same *stabilize factor* used in the symmetric case was employed. However, it was found that a higher value was required when thinner membranes were analysed.

6.2. Wrinkle details. Figure 14 shows the deformed shape of the membrane subjected to $T_1 = T_2 = 5$ N. The wrinkle pattern is symmetrical, like the loading, and the wrinkle amplitudes were found to be very small in this case. In the figure, the out-of-plane deformation, in the z-direction, has been magnified 100 times for the wrinkle details to show clearly.

Three asymmetric load cases were then considered: $T_1 = 10, 15, 20$ N, with $T_2 = 5$ N. The shape under the final loading is shown in Figure 15, and it is significantly different from that in Figure 14; a continuous, large diagonal wrinkle goes between the two more heavily loaded corners. In addition to this diagonal wrinkle, fans of small wrinkles can still be seen near the other two corners. The out-of-plane displacements in this plot have been amplified 10 times, for clarity.

The transition from the wrinkled shape shown in Figure 14 to that of Figure 15 is gradual, as can be seen from the contour plots of the out-of-plane displacements for increasing T_1/T_2, shown in Figure 16.

The initial pattern, shown in Figure 16 (top), is almost perfectly symmetric. It consists of four, practically identical fans of 9 wrinkles, one at each corner. Within each fan, each wrinkle subtends approximately the same angle, but the central

wrinkles have greater amplitude than the edge ones. Note that the wrinkle heights above and below the membrane are approximately equal.

When T_1 is increased to 10 N, the fans of wrinkles at the top left and bottom right corners become longer and deeper (see second panel in Figure 16), but the number of wrinkles in each fan is still 9. The wrinkle heights above and below the membrane continue to be approximately equal. The wrinkles at the other two corners become smaller in both amplitude and number.

When T_1 is increased to 15 N, the top left and bottom right fans merge and three diagonal wrinkles (down-up-down) go through the middle of the membrane. Note that the maximum wrinkle height above the membrane is now $+0.4$ mm, but below the membrane it is now -0.25 mm.
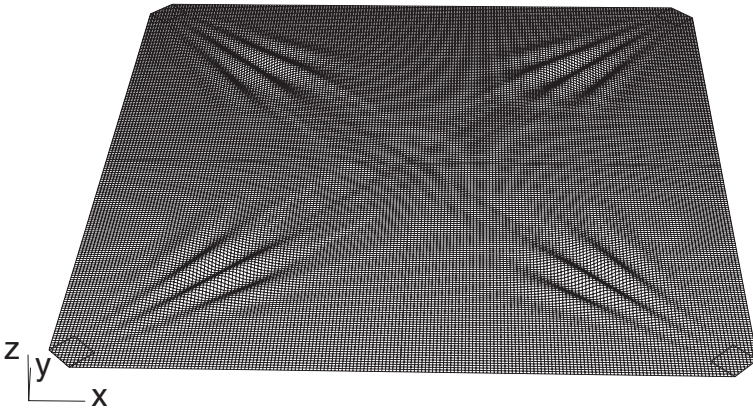
Figure 14. Wrinkled shape for $T_1 = T_2 = 5$ N (amplified 100 times).
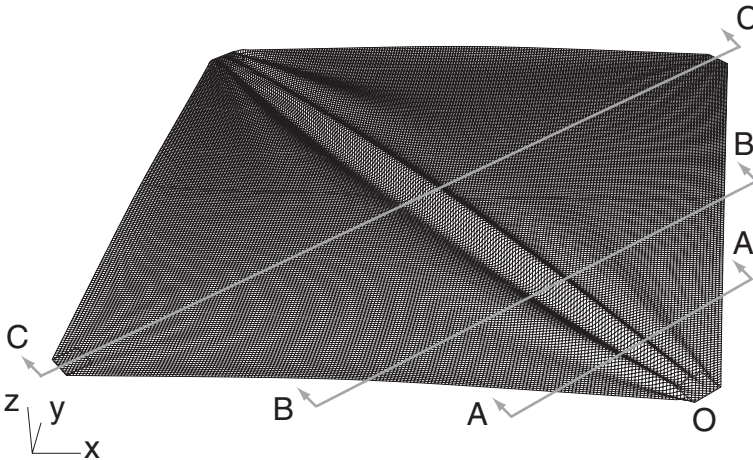
Figure 15. Wrinkled shape for $T_1 = 20$ N and $T_2 = 5$ N (amplified 10 times).
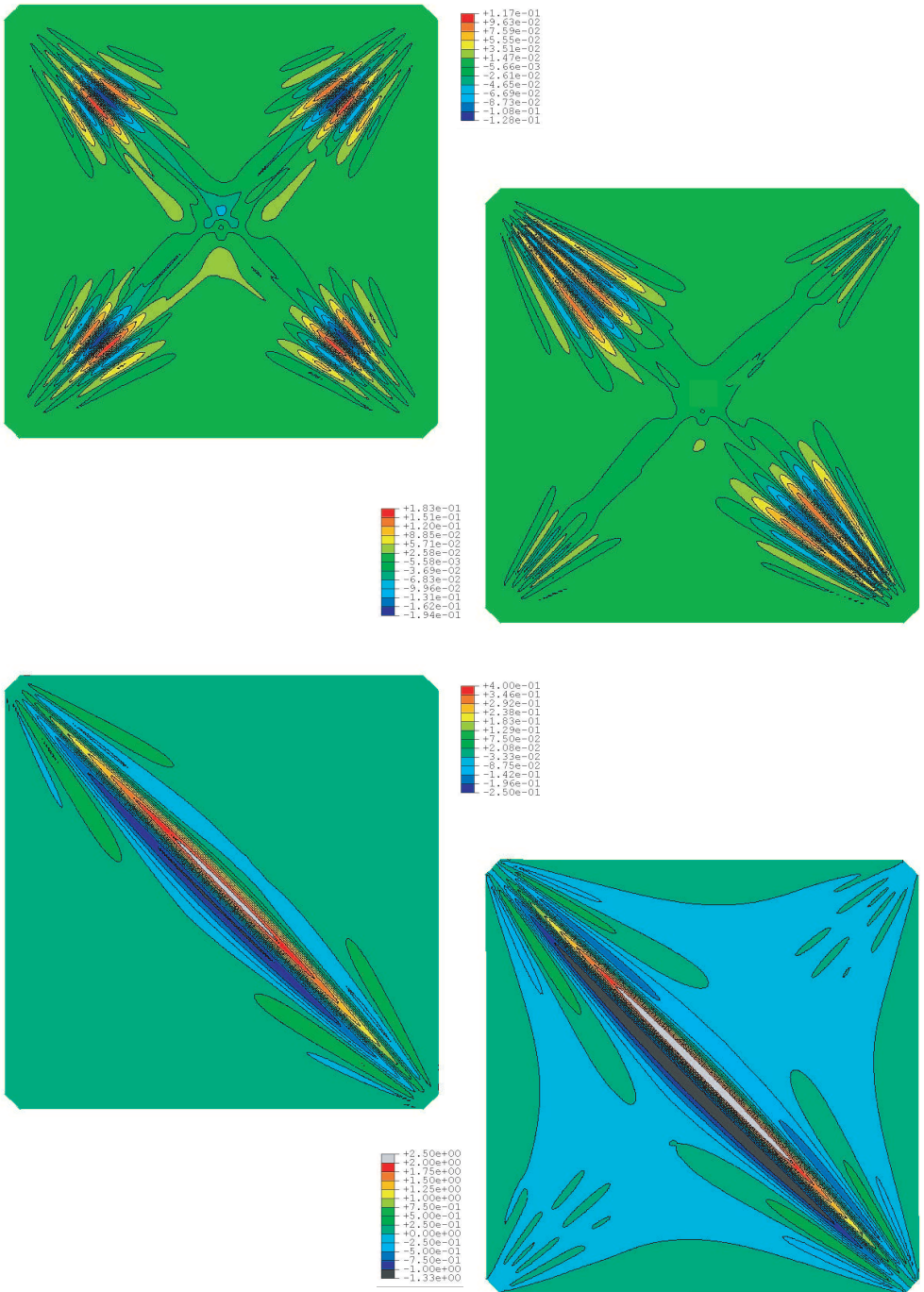
Figure 16. Contours of out-of-plane displacement for $T_2 = 5$ N and (from top to bottom) $T_1 = 5$ N, 10 N, 15 N, 20 N.

Finally, when T_1 is increased to 20 N (bottom panel in Figure 16), the diagonal wrinkles increase in amplitude, approximately five times, while maintaining the down-up-down profile. The wrinkles in the other corners increase in amplitude.

To analyse the final shape of the membrane in more detail, the out-of-plane displacements at three cross-sections (A-A, B-B and C-C in Figure 15) have been plotted in Figure 17. In addition to the three cross-sectional deformation plots obtained from the simulation, the figure shows also the experimental measurements from [Wong and Pellegrino 2006a].

Experiments and simulations match closely in the central region, and particularly the wrinkle wavelengths have been captured accurately. Gravity was included in the numerical simulations, to better capture the deformation of the edges; however, Figure 17(a-b) shows that the simulation still underpredicts the displacements of the edges of the membrane.

6.3. *Effects of load magnitude on wrinkles.* This section considers the variation of the wrinkle details with the magnitude of the applied loads. Figure 18(a) compares the cross-section at a distance of 105 mm from point O, which is roughly where the maximum displacements occur, for the case $T_1 = T_2 = 5$ N with the case $T_1 = T_2 = 20$ N. As can be seen, the wrinkle amplitudes increase, but the wavelength does not change.

Figure 18(b) compares the central cross-section, at a distance of 355 mm from point O, for the case $T_1 = 20$ N, $T_2 = 5$ N with the case $T_1 = 40$ N, $T_2 = 10$ N. Note that the wrinkle wavelength decreases when the applied load is increased. Also note that the small downwards wrinkle almost disappears, leaving an almost antisymmetric down-up wrinkle.

6.4. *Stress distribution.* Figure 19 shows the distribution of major midplane principal stresses in the membrane, for the four load ratios. The stress limits were set at 6.0 and 0 N/mm^2 in order to better visualize the stress variation. The general trend is that the stress decreases as one moves away from the corners of the membrane. For $T_1/T_2 = 1$ — see Figure 19(a) — the higher stresses are localized near the four corners, but for increasing T_1/T_2 the larger major principal stresses tend to spread along the main diagonal.

Because wrinkling is associated with the existence of (small) compressive stresses, it is instructive to consider also the distribution of the minor principal stresses, shown in Figure 20. The thin-shell model allows these stresses to become negative. For ease of comparison, the maximum and minimum stress limits were set at 1.0 and -2.0 N/mm^2. The key things to note are: (i) for $T_1/T_2 = 1$ — see Figure 20(a) — there are four identical regions of negative stress; (ii) two of these regions become smaller for $T_1/T_2 = 2$ and 3, while the other two regions grow bigger and
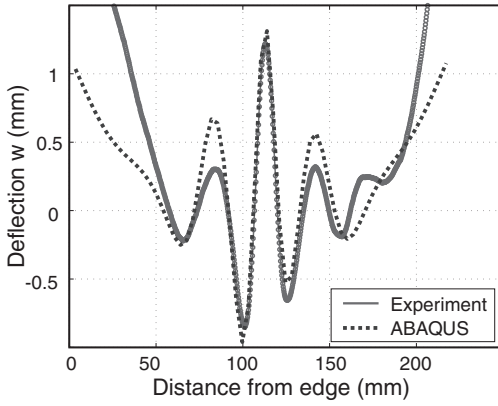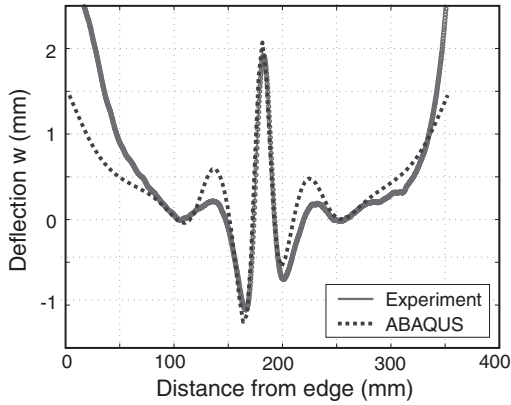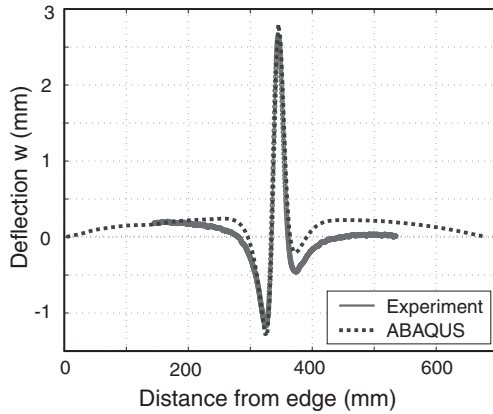
Figure 17. Experimental measurements with ABAQUS results for cross-sections at distances (a) 105 mm, (b) 177 mm, (c) 355 mm from the corner, for $T_1 = 20$ N and $T_1 = 5$ N.

coalesce in Figure 20(c); (iii) for $T_1/T_2 = 4$ the regions of compressive stress near the corners with the smaller loads have grown bigger.

7. Discussion and conclusion

A finite element simulation of wrinkled foils has been carried out with the commercial package ABAQUS, and the accuracy of the resulting wrinkle patterns has been demonstrated for two different problems. A key feature of the present approach is
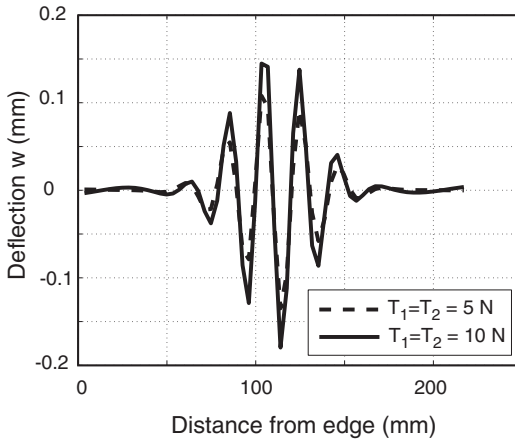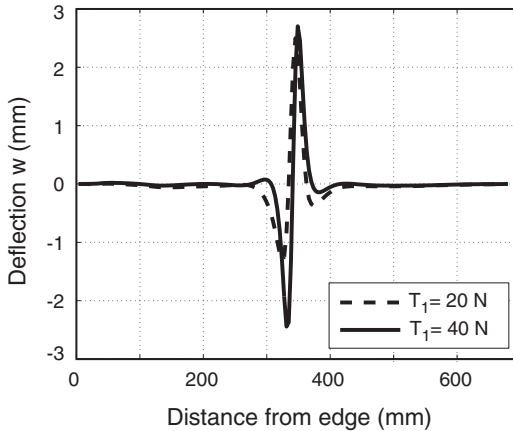

Figure 18. Variation of wrinkle profiles with load; (a) section at 105 mm from corner, for symmetric loads; (b) section at 355 mm from corner, for asymmetric loads with a ratio of 4.

that the geometrical imperfections that are seeded in the initially flat foil were obtained by computing the initial buckling modes of a perfectly flat foil that is lightly prestressed, to avoid highly localised buckling modes. This approach follows established, standard practice for the simulation of the post-buckling behaviour of imperfection-sensitive structures, and it has been shown that the experimentally observed behaviour of the foil is accurately captured.

The reduced integration shell elements available in ABAQUS have been found best suited to handle the combination of in-plane and bending behaviour associated with wrinkling, and element S4R5 was selected for speed of computation and accuracy. A mesh density of about 6 elements over a complete wrinkle wave, of length 2λ, was found sufficient to obtain accurate results. Further details on the analysis
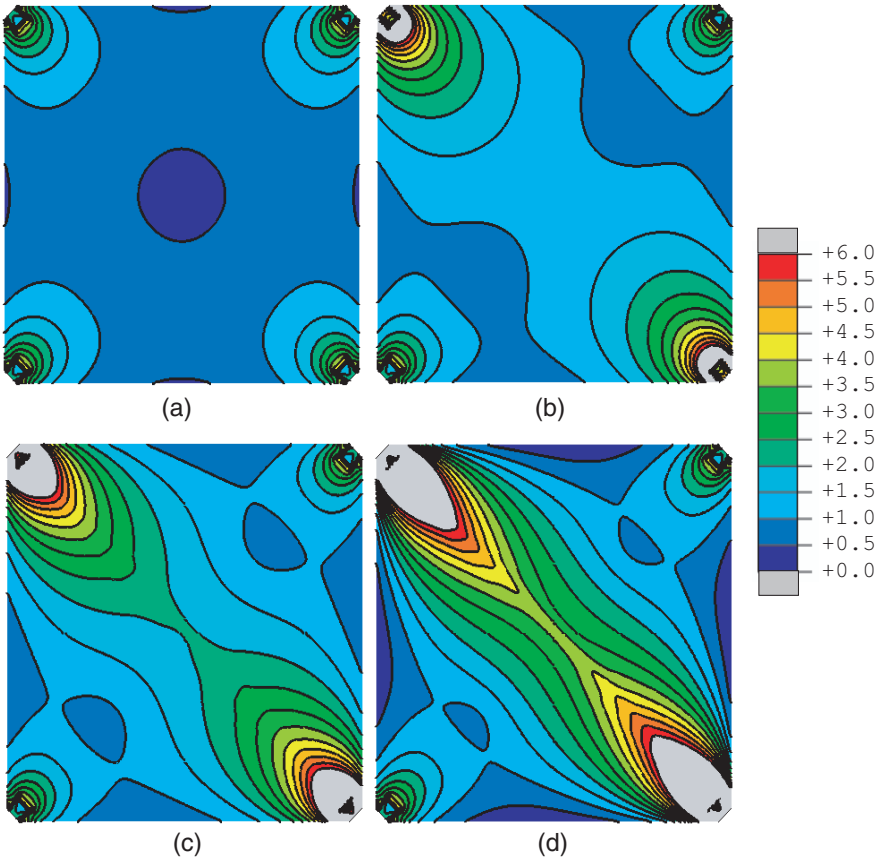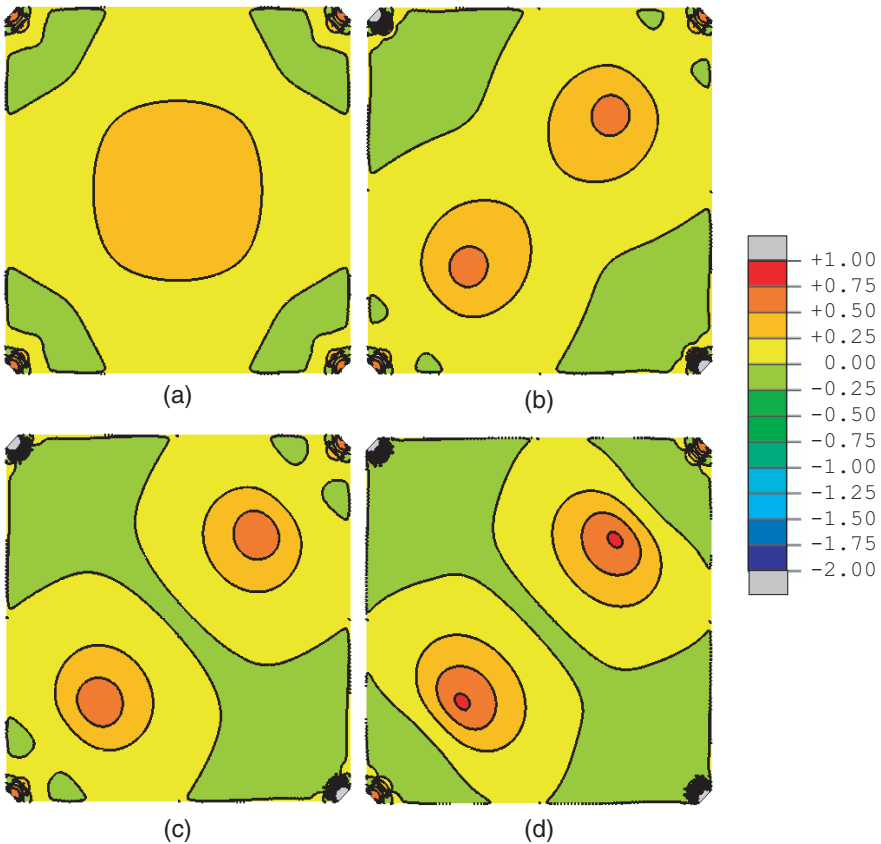

Figure 19. Contours of major midplane principal stress (in N/mm^2) obtained from thin-shell model for (a) $T_1 = T_2 = 5$ N; (b) $T_1 = 10$ N, $T_2 = 5$ N; (c) $T_1 = 15$ N, $T_2 = 5$ N; (d) $T_1 = 20$ N, $T_2 = 5$ N.

presented in this paper, including a sample ABAQUS input file, are available in
Wong [2003].

In cases where a preliminary analytical estimate of the smallest value of λ is
available, this estimate can be used to design a suitable finite element mesh. In other
cases, the mesh density has to be refined iteratively until the resulting distribution
of wrinkles has converged.

Our predictions are very accurate for the internal region of the foil, but it has
been noted that the free edges tend to move about 50% more than predicted by
the simulations. This may be due to the initial curling of the edges of Kapton®
foil (due to residual stresses resulting from manufacturing), compounded by the
fact that the free edges are practically unstressed, and hence "slack". Out-of-plane

Figure 20. Contours of minor midplane principal stress (in
N/mm^2) obtained from thin-shell model for (a) $T_1 = T_2 = 5$ N;
(b) $T_1 = 10$ N, $T_2 = 5$ N; (c) $T_1 = 15$ N, $T_2 = 5$ N; (d) $T_1 = 20$ N,
$T_2 = 5$ N.

displacements of slack membranes are notoriously ill-conditioned, and computing accurately the shape of a curled free edge would be even more extreme. An analysis specifically focussed on these effects, accompanied by additional experiments, will be required to shed more definitive light on this issue. From a practical standpoint, though, we have noted that edge deformations are often reduced very significantly if the free edges of a foil are cut on a slightly concave curve, instead of straight.

The sudden appearance or disappearance of new wrinkles, accompanied by the rearrangement (and change of wavelength) of the existing wrinkles — which were observed experimentally in [Wong and Pellegrino 2006a] — have been reproduced by our simulations. This behaviour has been understood as a form of mode-jumping, whose suddenness had been established in previous work by Stein [1959b] and Riks [1998]. Our simulations of load-cycling, in Figure 12, have shown that corresponding forward and reverse mode jumps occur at different displacements. This behaviour could be explained in terms of the shape of the equilibrium path of the structure, however, because the present displacement-controlled simulations were not able to trace unstable parts of the equilibrium path, at this stage it cannot be excluded that the behaviour in Figure 12 is an artefact of the type of solution procedure used in the present study.

Finally, it is noted that the present simulations have confirmed the existence of a small, compressive midsurface stress in a wrinkled foil. This was a fundamental assumption for the simple analytical model proposed in [Wong and Pellegrino 2006b].

Acknowledgements

References

[ABAQUS 2001] *ABAQUS theory and user's manual*, Version 6.2, Hibbitt Karlsson Sorensen Inc., Pawtucket, RI, 2001.

[Adler 2000] A. L. Adler, *Finite element approaches for static and dynamic analysis of partially wrinkled membrane structures*, PhD Dissertation, University of Colorado, Boulder, 2000.

[ANSYS 2000] *ANSYS User Manual*, version 5.7, ANSYS, Canonsburg, PA, 2000.

[Barsotti and Ligaro 2000] R. Barsotti and S. S. Ligaro, "An accurate wrinkled membrane model for analysing the post-critical behaviour of stiffened plate-girders", in *IASS-IACM 2000 Computational Methods for Shell and Spatial Structures*, edited by M. Papadrakakis et al., 2000.

[Contri and Schrefler 1988] P. Contri and B. A. Schrefler, "A geometrically nonlinear finite element analysis of wrinkled membrane surfaces by a no-compression material model", *Comm. Appl. Numer. Methods* **4** (1988), 5–15.

[Friedl et al. 2000] N. Friedl, F. G. Rammerstorfer, and F. D. Fischer, "Buckling of stretched strips", *Comput. Struct.* **78** (2000), 185–190.

[Haseganu and Steigmann 1994] E. M. Haseganu and D. J. Steigmann, "Analysis of partly wrinkled membranes by the method of dynamic relaxation", *Comput. Mech.* **14** (1994), 596–614.

[Johnston 2002] J. D. Johnston, "Finite element analysis of wrinkled membrane structures for sunshield applications", in *43rd AIAA/ASME/ASCE/AHS/ASC Structures, Structures Dynamics and Material Conference and Exhibit* (Denver, CO), 2002. AIAA-2002-1369.

[Kang and Im 1997] S. Kang and S. Im, "Finite element analysis of wrinkling membranes", *J. Appl. Mech.* **64** (1997), 263–269.

[Leifer and Belvin 2003] J. Leifer and W. K. Belvin, "Prediction of wrinkle amplitudes in thin fil membranes using finite element modeling", in *44th AIAA/ASME/ASCE/AHS/ASC Structures, Structural Dynamics and Materials Conference* (Norfolk, VA.), 7–10 April 2003 2003. AIAA 2003-1983.

[Lin and Mote 1996] C. C. Lin and C. D. Mote, "The wrinkling of rectangular webs under nonlinearly distributed edge loading", *J. Appl. Mech.* **63** (1996), 655–659.

[Liu et al. 1998] X. Liu, C. H. Jenkins, and W. W. Schur, "Computational issues in the modelling of wrinkling during parachute deployment", pp. 239–250 in *IUTAM-IASS Symposium on Deployable Structures: Theory and Application*, edited by S. Pellegrino and S. D. Guest, Kluwer, 1998.

[Liu et al. 2000] X. Liu, C. H. Jenkins, and W. W. Schur, "Fine scale analysis of wrinkled membranes", *Int. J. Comput. Eng. Sci.* **1** (2000), 281–298.

[Liu et al. 2001] X. Liu, C. H. Jenkins, and W. W. Schur, "Large deflection analysis of pneumatic envelopes using a penalty parameter modified material model", *Finite Elem. Anal. Des.* **37** (2001), 233–251.

[Miller and Hedgepeth 1982] R. K. Miller and J. M. Hedgepeth, "An algorithm for finite element analysis of partly wrinkled membranes", *AIAA Journal* **20** (1982), 1761–1763.

[Miller et al. 1985] R. K. Miller, J. M. Hedgepeth, V. I. Weingarten, P. Das, and S. Kahyai, "Finite element analysis of partly wrinkled membranes", *Comput. Struct.* **20** (1985), 631–639.

[Nakashino and Natori 2005] K. Nakashino and M. C. Natori, "Efficient modification scheme of stress-strain tensor for wrinkled membranes", *AIAA Journal* **43** (2005), 206–215.

[Papa and Pellegrino 2005] A. Papa and S. Pellegrino, "Mechanics of systematically creased thin-film membrane structures", in *46th AIAA/ASME/ASCE/AHS/ASC Structures, Structural Dynamics and Materials Conference* (Austin, TX), 2005. AIAA 2005-1975.

[Riks 1998] E. Riks, "Buckling analysis of elastic structures: a computational approach", *Adv. Appl. Mech.* **34** (1998), 1–76.

[Roddeman et al. 1987] D. G. Roddeman, J. Drukker, C. W. J. Oomens, and J. D. Janssen, "The wrinkling of thin membranes: Part II–Numerical Analysis", *J. Appl. Mech.* **54** (1987), 888–892.

[Stein 1959a] M. Stein, "Loads and deformations of buckled rectangular plates", NASA, 1959, Available at http://hdl.handle.net/2002/10499.

[Stein 1959b] M. Stein, "The phenomenon of change of buckling patterns in elastic structures", NASA, 1959, Available at http://hdl.handle.net/2002/10498.

[Tessler and Sleight 2004] A. Tessler and D. W. Sleight, "Toward effective shell modeling of wrinkled thin-film membranes exhibiting stress concentrations", in *45th AIAA/ASME/ASCE/AHS/ASC*

Structures, Structural Dynamics and Materials Conference (Palm Springs, CA), 2004. AIAA 2004-1739.

[Tessler et al. 2003] A. Tessler, D. W. Sleight, and J. T. Wang, "Nonlinear shell modeling of thin membranes with emphasis on structural wrinkling", in *44th AIAA/ASME/ASCE/AHS/ASC Structures, Structural Dynamics and Materials Conference* (Norfolk, VA), 2003. AIAA 2003-1931.

[Tessler et al. 2005] A. Tessler, Sleight, D. W., and J. T. Wang, "Effective modeling and nonlinear shell analysis of thin membranes exhibiting structural wrinkling", *J. Spacecraft Rockets* **42**:2 (2005), 287–298.

[Tomita and Shindo 1988] Y. Tomita and A. Shindo, "Onset and growth of wrinkles in thin square plates subjected to diagonal tension", *Int. J. Mech. Sci.* **30** (1988), 921–931.

[Wong 2003] Y. W. Wong, *Wrinkling of thin membranes*, Ph.D. thesis, University of Cambridge, 2003.

[Wong and Pellegrino 2002a] Y. W. Wong and S. Pellegrino, "Computation of wrinkle amplitudes in thin membranes", in *43rd AIAA/ASME/ASCE/AHS/ASC Structures, Structures Dynamics and Material Conference and Exhibit* (Denver, CO), 2002a. AIAA-2002-1369.

[Wong and Pellegrino 2006a] Y. W. Wong and S. Pellegrino, "Wrinkled membranes I: experiments", *J. of Mechanics of Materials and Structures* **1** (2006), 3–25.

[Wong and Pellegrino 2006b] Y. W. Wong and S. Pellegrino, "Wrinkled membranes II: analytical models", *J. of Mechanics of Materials and Structures* **1** (2006), 27–61.

[Wong et al. 2003] Y. W. Wong, S. Pellegrino, and K. C. Park, "Prediction of wrinkle amplitudes in square solar sails", in *44th AIAA/ASME/ASCE/AHS/ASC Structures, Structural Dynamics and Materials Conference and Exhibit*, 2003. AIAA-2003-1980.

Y. WESLEY WONG: wesleywong@cantab.net

SERGIO PELLEGRINO: pellegrino@eng.cam.ac.uk
Department of Engineering, University of Cambridge, Trumpington Street, Cambridge, CB2 1PZ, United Kingdom